https://doi.org/10.5194/egusphere-2024-103
Preprint. Discussion started: 19 February 2024

NO_x emissions in France in 2019-2021 as estimated by the high spatial resolution assimilation of TROPOMI NO_2 observations

Robin Plauchu [1], Audrey Fortems-Cheiney [1,*], Grégoire Broquet [1], Isabelle Pison [1], Antoine Berchet [1], Elise Potier [1,**], Gaëlle Dufour [2], Adriana Coman [3], Dilek Savas [2], Guillaume Siour [3], and Henk Eskes [4]

[1]Laboratoire des Sciences du Climat et de l'Environnement, LSCE/IPSL, CEA-CNRS-UVSQ, Université Paris-Saclay, F-91191 Gif-sur-Yvette, France
[2]Université Paris Cité and Univ Paris Est Créteil, CNRS, LISA, F-75013 Paris, France
[3]Univ Paris Est Créteil and Université Paris Cité, CNRS, LISA, F-94010 Créteil, France
[4]Royal Netherlands Meteorological Institute (KNMI), De Bilt, the Netherlands
[*]Now in Science Partners, Quai de Jemmapes, 75010 Paris, France
[**]Now in Université Paris Cité and Univ Paris Est Créteil, CNRS, LISA, F-75013 Paris, France

Correspondence to: Robin Plauchu (robin.plauchu@lsce.ipsl.fr)

Abstract.

Since 2018, TROPOMI on-board Sentinel-5P provides unprecedented images of NO_2 tropospheric columns at a relatively high spatial resolution with a daily revisit. This study aims at assessing the potential of the TROPOMI-PAL data to estimate the national to urban NO_x emissions in France from 2019 to 2021, using the variational mode of the recent Community Inversion Framework coupled to the CHIMERE regional transport model at a spatial resolution of 10×10 km^2. The seasonal to inter-annual variations of the NO_x French emissions are analyzed. A specific attention is paid to the current capability to quantify strong anomalies in the NO_x emissions at intra-annual scales such as the ones due to the COVID-19 pandemic, by using TROPOMI NO_2 observations.

The inversions lead to a decrease of the average emissions over 2019-2021 compared to 2016 of -3% at national scale, which is lower than the decrease of -14% between these years in the estimates of the French Technical Center for Air Pollution and Climate Change (CITEPA). This may be linked especially to the limited level of constraint brought by the TROPOMI data, due to the observation coverage and the ratio between the current level of errors in the observation and the chemistry-transport model, and the NO_2 signal from the French anthropogenic sources.

Focusing on local analysis and selecting the days during which the TROPOMI coverage is good over a specific local source, we compute the reductions in the NO_x anthropogenic emission estimates by the inversions from spring 2019 to spring 2020. These reductions are particularly pronounced for the largest French urban areas (e.g., -26% from April 2019 to April 2020 in the Paris urban area), consistently with the reduction in the intensity of vehicle traffic reported during the lockdown period.

https://doi.org/10.5194/egusphere-2024-103
Preprint. Discussion started: 19 February 2024

1 Introduction

Emitted mainly by road traffic, thermal power plants and industrial activities and produced in the atmosphere by the oxidation of nitric oxide (NO), which is emitted by the same activities, nitrogen dioxide (NO_2) is of great interest due to its important role in many atmospheric processes with strong implications for air quality, health, climate change and ecosystems. It is one of the major air pollutants with adverse impact on health (Costa et al., 2014; EEA, 2020). Deposition of nitrogen compounds like nitrates, for which NO_2 is a precursor, leads to eutrophication of ecosystems (Stevens et al., 2018). NO_2 also indirectly affects the radiative forcing as a precursor of tropospheric ozone and particulate matter. NO_2 is therefore one of the regulated air quality pollutants. Nevertheless, despite ongoing improvements in the overall air quality, levels of air pollutants above standards of the European Union (UE) are still measured across Europe and air pollution remains a major health concern for European citizens (EEA, 2023). For example, France was condemned in 2019 by the Court of Justice of the EU (CJEU) for non-compliance with Directive 2008/50/EC relating to ambient air quality, and more specifically for exceeding systematically and persistently concentration limit values (CLV, 40 $\mu g.m^{-3}$ on annual average) for NO_2, particularly in the Ile-de-France area, close to traffic. According to Airparif (2022), the planned reductions in the emissions of nitrogen oxides (NO_x=NO+NO_2) will still be insufficient by 2025 to respect the NO_2 CLV, which should have been reached with since January 2010.

The society is thus faced with a major environmental challenge: the need to rapidly reduce NO_2 concentrations to levels that comply with the law (EU Directive 2016/2284) and do not impact human health or ecosystems and therefore to reduce anthropogenic NO_x emissions. An accurate account of NO_x emissions in space and time is needed to assess the effectiveness of policies aiming at reducing NO_x emissions. However, the quantification of anthropogenic NO_x emissions following a bottom-up (BU) approach, based on the statistics of activity sectors and fuel consumption and relying on emission factors per activity type, suffer from relatively large uncertainties. For example, at national and annual scales, these uncertainties reach 50-200% depending on the activity sector in the European Monitoring and Evaluation Programme (EMEP) inventory (Kuenen and Dore, 2019) and these emission factors can be biased (e.g., with the Dieselgate, Brand (2016)). In addition, the use of proxies and typical temporal profiles inevitably introduces errors in the quantification of the spatio-temporal variability at high resolutions. In situ information could be used to analyze local emissions and their variations due to specific events or measures (Guevara et al., 2023). Finally, the BU inventories are often delivered with a 2-year lag. The assessment of AQ (Air Quality) policies (as mentioned above) would benefit from accurate emission inventories spatialized at a high resolution with a fast update capability and integrating independent information could play a critical role for the AQ analysis and policies. The use of atmospheric measurements to complement current BU approaches may then support the development of such inventories.

Since the 2000s, NO_2 atmospheric mixing ratios have been monitored around the world by space-borne instruments, such as the Global Ozone Monitoring Experiment GOME (Burrows et al., 1999) and GOME-2 (Munro et al., 2016), the SCanning Imaging Absorption spectroMeter for Atmospheric CHartographY SCIAMACHY (Burrows et al., 1995; Bovensmann et al., 1999) and the Ozone Monitoring Instrument OMI (Levelt et al., 2018).

In this context, attempts have been made to develop so-called top-down (TD) methods, complementary to BU inventories, to deduce NO_x emissions from NO_2 satellite data. These methods are based on the principle that atmospheric levels and variations

https://doi.org/10.5194/egusphere-2024-103
Preprint. Discussion started: 19 February 2024

of NO_2 reflect the convolution of the amplitude and variations of NO_x emissions with the atmospheric chemistry and physics. Through the statistical inverse modeling of the atmospheric chemistry and transport, one can derive estimates of the emissions based on the concentration fields. However, strong non-linear relationships exist between NO_x emissions and satellite NO_2 tropospheric vertical column densities (TVCDs) (Lamsal et al., 2011; Vinken et al., 2014; Miyazaki et al., 2017; Elguindi et al., 2020) due to the complex chemistry affecting NO_x in the atmosphere.

This complex atmospheric chemistry has been taken into account in various ways in more or less complex TD methods. Mass–balance approaches have been performed at the global (Lamsal et al., 2011; Vinken et al., 2014) and regional (Visser et al., 2019) scales, accounting for non-linear relationships between NO_x emission changes and NO_2 TVCDs via reactions with hydroxyl radicals (OH) but with simple scaling factors. However, Stavrakou et al. (2013) have shown that other direct or indirect NO_x sinks associated with other species (such as ozone O_3 or the HO_2 radical) could significantly influence NO_2 concentrations in the atmosphere and therefore TD estimates. A more detailed account of the complex NO_x chemistry should thus support more accurate derivations of NO_x emissions from NO_2 satellite data. Therefore, more elaborated approaches using chemistry transport models (CTM) with ensemble Kalman filter inverse modeling techniques or variational approaches, have been used to infer NO_x emissions at the global (Müller and Stavrakou, 2005; Miyazaki et al., 2017) or at the regional scale (van der A et al., 2008; Mijling and van der A, 2012; Mijling et al., 2013; Lin, 2012; Ding et al., 2017; Savas et al., 2023). However, NO_x inversions from satellite NO_2 observations have resolution-dependent biases: coarse-resolution models are known to bear negative biases in NO_2 over large sources (Valin et al., 2011). It would be therefore essential to operate at finer spatial resolutions. In addition, monitoring NO_x emissions implies monitoring hotspots of emissions (large urban and industrial areas or strong point sources), which concentrate much of the global emissions (57% of the global population lives in urban areas as of 2022, Ritchie and Roser (2018)). Being able to monitor individually emission hotspots is required to assess the emission reduction policies since the scales they target range from the regional scale (e.g., that of the EU) to the country scale or even to that of smaller territory units e.g., cities. This requires in turn a high spatial and temporal resolution mapping of NO_2 concentrations.

Since 2017, the TROPOspheric Monitoring Instrument (TROPOMI, Veefkind et al. (2012)) on-board the Copernicus Sentinel-5 Precursor (S5P) monitors atmospheric NO_2 with a high-resolution imaging (pixel size of about 5.6×3.6 km^2 since August 2019), which should support the quantification of anthropogenic emissions at national to local scales. With a swath as wide as approximately 2600 km on ground, the TROPOMI instrument also provides an unprecedented daily coverage. It theoretically covers any point of the Earth 1 to 2 times a day. The need for surface solar irradiance, the cloud cover and the quality filtering limit the number of pixels in numerous images locally (e.g., at high latitudes) but the possibility of having a follow-up week by week (even day by day) remains for large portions of the globe.

To fully exploit these TROPOMI satellite images, variational inversion systems seem particularly adapted since they allow for solving high-dimensional problems (Elbern et al., 2000; Quélo et al., 2005; Pison et al., 2009; Henze et al., 2009; Cao et al., 2022), typically addressing the emission fluxes at high spatial and temporal resolutions and assimilating a large number of data, such as provided in TROPOMI images. The non-linearities of the chemistry of NO_x can be dealt with in a variational inversion framework driving a regional CTM using a manageable chemistry scheme to simulate NO_2 concentrations and whose adjoint

https://doi.org/10.5194/egusphere-2024-103
Preprint. Discussion started: 19 February 2024

code is available.

In this context, this study assesses the potential of the TROPOMI observations to inform about NO_x emissions in France from 2019 to 2021 at national to urban scales. We use the high-dimensional variational inversion drivers of the recent Community Inversion Framework (CIF, Berchet et al. (2021)). The CIF drives a configuration of the CHIMERE regional CTM (Menut et al., 2013; Mailler et al., 2017) covering France at 10×10 km^2 spatial resolution, including a chemistry module taking into account the complex NO_x chemistry in gas-phase and its non-linearities, and of its adjoint (Fortems-Cheiney et al., 2021). This relatively fine spatial resolution makes it possible to focus on the French largest urban areas. The period 2019–2021 covers the phase of the COVID-19 crisis in spring 2020 during which NO_2 concentrations and NO_x anthropogenic emissions are expected to have significantly dropped over Europe (Bauwens et al., 2020; Menut et al., 2020; Diamond and Wood, 2020; Ordóñez et al., 2020; Petetin et al., 2020; Barré et al., 2021; Gaubert et al., 2021; Deroubaix et al., 2021; Lee et al., 2021; Souri et al., 2021; Levelt et al., 2022; Guevara et al., 2021, 2022, 2023). In France, the population has been confined from March 17^{th} to May 10^{th} and all public spaces deemed non-essential to daily life in the country have been shut down. Then, from May 11^{th} to June 1^{st}, lockdown restrictions have progressively been lifted. The population has been confined again from October 30^{th} to December 15^{th}. The analysis of the emissions from 2019–2021 should thus provide insights on the current capability to quantify strong anomalies in the NO_x emissions at intra-annual scales by using satellite NO_2 observations.

Our configuration of the CHIMERE CTM, the NO_2 TROPOMI satellite observations, and the variational inversion framework and set up are described in Section 2. Section 3 presents the results of our study, including comparisons between TROPOMI-PAL NO_2 TVCDs and their CHIMERE simulated equivalents and the analysis of the spatio-temporal variability of the French NO_x emissions. Our conclusions are given in Section 4.

https://doi.org/10.5194/egusphere-2024-103
Preprint. Discussion started: 19 February 2024

2 Data and method

2.1 Prior estimates of the emission maps

The principle of the inversion is to correct *a priori* emission maps later on referred as "prior emissions". The prior estimates of NO_x emissions in this study are based on the CAMS-REG inventory (Kuenen et al., 2022) for the year 2016, and on the Inventaire National Spatialisé (INS) inventory for the year 2012 (Institut National de l'Environnement industriel et des RISques - INERIS -, Ministry of Ecological Transition, hosted at http://emissions-air.developpement-durable.gouv.fr/index.html). The CAMS-REG inventory provides anthropogenic emissions at a 0.05°longitude × 0.1°latitude resolution. Anthropogenic emissions for non-methane volatile organic compounds (NMVOCs) emissions from CAMS-REG are accounted for in our simulations, but are not controlled by the inversions (see Section 2.5).

Annual and national budgets are based on the officially reported emission data by European countries to the Convention on Long-Range Transboundary Air Pollution and the EU National Emission Ceilings Directive. These budgets are then disaggregated in space based on proxies of the different sectors. Temporal disaggregation is based on temporal profiles provided per sector with typical month to month, weekday to week-end and diurnal variations (Ebel et al., 1997; Menut et al., 2012). Spatial proxies for point sources and areas sources described in Kuenen et al. (2022) are used to spatialize the emissions.

CAMS-REG provides not only the gridded emissions but also default profiles for typical emission height by source type (Kuenen et al., 2022), which accounts for the average effective emission height (including plume rise), based on Bieser et al. (2011). The spatialization for France is based on proxies of the INS on a municipal scale while the spatialization for the other countries within our modeling domain is directly taken as that of CAMS-REG. The inventory is therefore called "CAMS-REG/INS" in the following.

The natural NO_x emissions are prescribed using simulations from the Model of Emissions of Gases and Aerosols from Nature (MEGAN) model (Guenther et al., 2006), with a ~1×1 km^2 spatial resolution.

Lightning NO_x fluxes, whose impact on NO_2 concentrations is very small in Europe even in summer (Menut et al., 2020), are not accounted for. Fire emissions are also ignored, as we assume that they only slightly contribute to the NO_x total emissions. These emission maps have been aggregated to the grid of CHIMERE for the years 2019 to 2021 (Section 2.2 and Figure 1).

2.2 Configuration of the CHIMERE CTM

We use the CHIMERE v2013 model to simulate fields of concentrations of gaseous chemical species in a domain that covers France and its vicinity (11°W-12°E; 39.5°N-54.5°N, see Figure 1). The model horizontal grid is zoomed (Siour et al., 2013), with a 10-km resolution regular sub-grid in the center of the domain covering the full France and a 50-km resolution in the corners of the domain (Figure 1). It corresponds to 166 (longitude) × 122 (latitude) horizontal grid cells. The model has 20 vertical layers, from the surface to 200 hPa, with 8 layers within the first two kilometers.

The model is driven by the European Centre for Medium-Range Weather Forecasts (ECMWF) global meteorological fields (Owens and Hewson, 2018). Both CHIMERE (Menut et al., 2013) and its adjoint code operate the MELCHIOR-2 chemical scheme, with more than 100 reactions (Lattuati, 1997; Derognat et al., 2003), including 24 for inorganic chemistry. Con-

https://doi.org/10.5194/egusphere-2024-103
Preprint. Discussion started: 19 February 2024

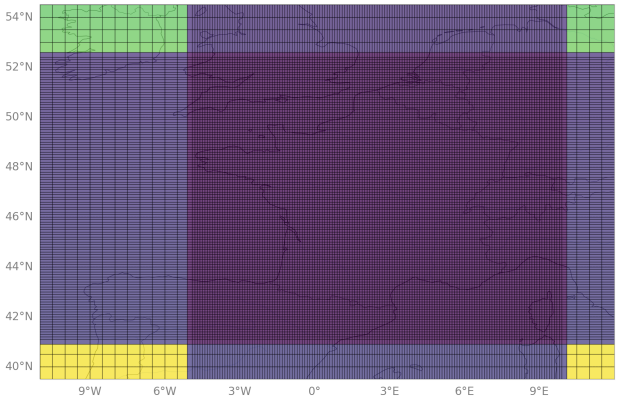

Figure 1. *Domain of our CHIMERE configuration: 10-*km *resolution regular sub-grid in purple, 50-*km *resolution in green and yellow, 10×50* km *resolution in blue.*

sidering the NO_2 short lifetime, we do not consider its import from outside the domain: its boundary conditions are set to zero. Nevertheless, the lateral and top boundaries for other species such as ozone O_3, nitric acid HNO_3, peroxyacetyl nitrate PAN, formaldehyde HCHO, participating to the NO_x chemistry, are taken into account. Initial and boundary conditions when relevant are specified using a nested run of CHIMERE (Siour et al., 2013) over a European domain (15.25°W-35.75°E; 31.75°N-74.25°N) with a spatial resolution of 0.5°, using itself boundary and initial conditions from climatological values from the LMDZ-INCA global model (Szopa et al., 2009).

The aerosol module of CHIMERE is not considered in the simulations and inversions, as the adjoint of this module is not available (Fortems-Cheiney et al., 2021; Savas et al., 2023).

2.3 TROPOMI-PAL observations

TROPOMI, launched onboard Sentinel 5 Precursor in October 2017, is in a near-polar sun-synchronous orbit (approximate altitude of ~824 km) with an ascending node equatorial crossing at ~13h40 Mean Local Solar time. With an orbital cycle of 16 days, and 14 orbits a day, the satellite passes over the same geographical area every cycle of 227 orbits. With a swath as wide as 108°— approximately 2600 km on ground — TROPOMI provides daily coverage for NO_2. Observations over our domain span from around 9:30 am to 2:30 pm local time with data from 2 to 3 orbits per day, with the major coverage around noon (11:30 am to 1:30 pm).

An evaluation of the TROPOMI-v1.3 product with surface remote sensing observations had indicated a systematic low bias of TROPOMI NO_2 tropospheric vertical columns densities (TVCDs) of typically -23% to -37% in clean to slightly polluted conditions and as high as -51% over highly polluted areas (Verhoelst et al., 2021) compared to ground-based measurements. This negative bias has been mainly attributed to a negative cloud height bias in the Fast Retrieval Scheme for Clouds from Oxygen absorption band (FRESCO) implementation (van Geffen et al., 2022b) and efforts have been made to correct it in the TROPOMI-PAL product (Eskes et al., 2021).

https://doi.org/10.5194/egusphere-2024-103
Preprint. Discussion started: 19 February 2024

Here, we use the PAL TROPOMI reprocessed data (Eskes et al., 2021), available from 2019 to the 11^{th} of November, 2021. We use a recent reprocessing of the TROPOMI data, called RPRO version 2.4, to cover the end of the year 2021. This latest reprocessing uses a new higher-resolution directional Lambertian-equivalent reflectivity derived from TROPOMI observations (van Geffen et al., 2022a). Nevertheless, the last evaluation of the TROPOMI RPRO v2.4 product with surface remote sensing observations still indicates significant biases of TROPOMI the NO_2 TVCDs of typically +13% over clean areas to -40% over highly polluted areas (Lambert et al., 2023). Part of theses biases could be explained by the relatively coarse horizontal resolution of the gloabl TM5-MP prior profiles ($1° \times 1°$) used in the retrieval process (which can be neglected when applying the retrieval averaging kernels to the model) (Douros et al., 2023). However, these biases are also largely attributed to systematic errors in the retrieved cloud pressure, surface albedo used etc. (Boersma et al., 2016; Douros et al., 2023).

We select the data with a quality assurance (qa) value of 0.75 for both products, following the criteria of van Geffen et al. (2022b). The latest version of the TROPOMI NO_2 Algorithm Theoretical Basis Document (ATBD) is now for product version 2.6 (TROPOMI ATBD of the total and tropospheric NO_2 data products, KNMI, S5P-KNMI-L2-0005-RP, issue 2.4.0, van Geffen et al. (2022a)).

2.4 Comparison between simulated and observed NO_2 TVCDs

To make relevant comparisons between simulations and satellite observations, the averaging kernels (AKs), which are associated with each observed TVCD and representing the vertical sensitivity of the satellite retrieval (Eskes and Boersma, 2003) are applied to the simulated concentration field. Due to the over-sampling resulting from the model's horizontal resolution being coarser than the TROPOMI data, we aggregate spatially and temporally the TROPOMI observations at the CHIMERE resolution into so-called super-observations. Within a given grid cell and time step, the super-observation is the observation (TVCD and AKs) which is the closest to the mean of the TROPOMI TVCDs. The error associated with each super-observation is also derived from the observation closest to the mean value and subsequently included into the total so-called "observation error" (see Section 2.5). Our derivation of the error associated with each super-observation is thus conservative compared to other studies (Boersma et al., 2016) where the super-observation uncertainty is reduced compared to that of individual observations. The reduction of uncertainty when combining several observations account for the fact that the retrieval errors include random noise (in particular, instrumental noise) without spatial correlation, i.e. errors which are independent from one observation to the other. However, as discussed above, the TROPOMI NO_2 observations bear large systematic errors from the retrieval process, which can exhibit significant spatial correlations. This explains our conservative attribution of observation errors to the super-observations.

The corresponding column of NO_2 in CHIMERE is vertically interpolated (at TROPOMI's super-observation location) on the vertical levels of the super-observation retrieval, and vertically integrated with the AKs of the super-observation, to yield the NO_2 simulated TVCD to be compared to the super-observation TVCD, as illustrated in Figure 2a) and Figure 2b) for the month of April 2020.

https://doi.org/10.5194/egusphere-2024-103
Preprint. Discussion started: 19 February 2024

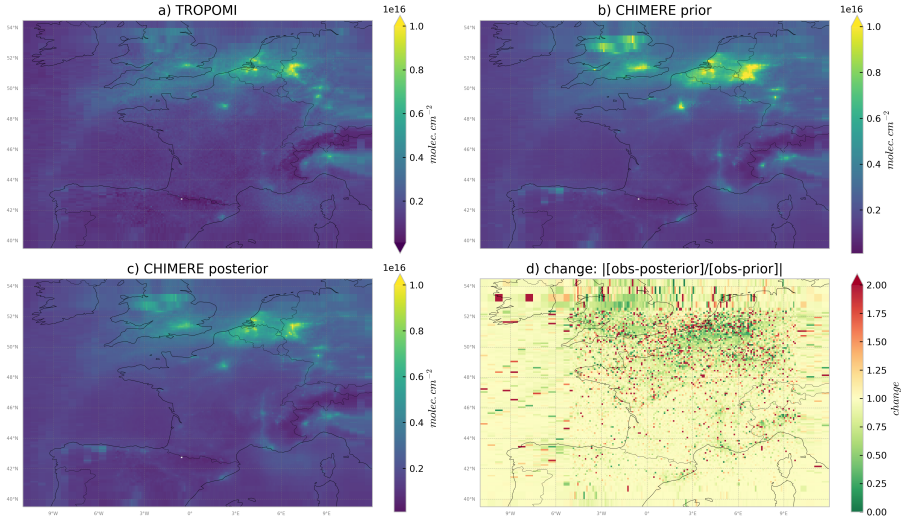

Figure 2. *Averages of NO_2 TVCDs by a) the TROPOMI-PAL data, b) the CHIMERE simulation using prior emissions from the CAMS-REG/INS and MEGAN inventories, described in Section 2.1 and c) the CHIMERE simulation using the posterior emissions from the inversion, for April 2020, in* $\mathrm{molec.cm}^{-2}$. *d) Ratio of the posterior and prior biases between NO_2 TVCDs simulated with CHIMERE and the TROPOMI-PAL observations. All ratios lower than 1, in green, demonstrate that posterior emission estimates improve the simulation compared to the prior ones.*

2.5 Variational inversion of NO_x emissions

The inversion of NO_x emissions consists in correcting the prior estimate of the emissions (presented in Section 2.1) to improve the fit between NO_2 TROPOMI-PAL satellite data and their simulated equivalents, using a Bayesian variational inversion framework similar to that of Fortems-Cheiney et al. (2021).

Series of 7-day inversion windows — independent from each other — are run and then combined to provide a corrected ("posterior") estimate of NO_x emissions over the whole period of analysis (2019-2021). For each inversion window, the posterior estimate of the emissions is found by iteratively minimizing the cost function $J(\mathbf{x})$:

$$J(\mathbf{x}) = (\mathbf{x}-\mathbf{x}^b)^T\mathbf{B}^{-1}(\mathbf{x}-\mathbf{x}^b) + (\mathcal{H}(\mathbf{x})-\mathbf{y})^T\mathbf{R}^{-1}(\mathcal{H}(\mathbf{x})-\mathbf{y}) \quad (1)$$

where $\mathbf{x}$, $\mathcal{H}$, $\mathbf{y}$, $\mathbf{B}$, $\mathbf{R}$ are respectively the control vector, the observation operator, the satellite observations, the prior error covariance matrix and the observation error covariance matrix. The control vector $\mathbf{x}$ gathers variables for the correction of the surface NO and NO_2 emissions, $\mathbf{x^b}$ corresponding to the prior estimate of the control vector. Contrarily to Fortems-Cheiney et al. (2021), we model the prior uncertainty in the NO_x emissions with a log-normal distribution. This allows the inversion system to apply high variations in NO_x emissions while ensuring positivity, unlike the classic corrections of the emission with scaling factors with a Gaussian distribution of prior uncertainty. We have introduced the random variable ψ following a normal

https://doi.org/10.5194/egusphere-2024-103
Preprint. Discussion started: 19 February 2024

distribution, for each type of emission, such that:

$$\begin{cases} \psi \sim N(0, \mathbf{B}) \\ emissions(\psi) = \exp(\mathbf{x}) \cdot emission_{prior} \end{cases} \tag{2}$$

Thus, our control vector $\mathbf{x}$ is defined as the ensemble of ψ for each type of emission (NO_2, NO) in our inversion.

Our control vector $\mathbf{x}$ therefore contains:

- the logarithms of the scaling coefficients for NO and NO_2 anthropogenic emissions at a 1-day temporal resolution, for the 166 (longitude) $\times$ 122 (latitude) horizontal grid cells, and over three vertical bands of injection heights for the emissions (the first 2 layers from 0 to 25 m, layers 3 to 10 from about 25 to 1900 m and layers 11 to 20 from about 1900 to 12000 m); this is done essentially to reduce the dimensionality of the problem along this axis as most emissions are concentrated in the first 2 layers. The corrections applied are the same for all layers within a band.
- the logarithms of the scaling coefficients for NO natural emissions at a 1-day temporal resolution, for the 166 (longitude) $\times$ 122 (latitude) grid cells at the surface level.

NO and NO_2 3D initial conditions (specified using a nested run of CHIMERE, as described in Section 2.2) are not controlled and are set once initially for all 7-day windows at 0:00 UTC on the first day of these windows. We therefore do not account for the potential update of the concentrations during a previous 7-day window due to the inversions. They have a low impact on the inversion since the first satellite observations over the domain are around noon while the NO_x lifetime is short (of the order of one day).

The uncertainties in the observations y together with that in the observation operator $\mathcal{H}$, and the uncertainties in the prior estimate of the control vector $\mathbf{x^b}$ are assumed to have a Gaussian distribution. Here, the prior error covariance matrix $\mathbf{B}$ is block diagonal (see Equation 3). The first block corresponds to the logarithms of the anthropogenic fluxes factors. We assume that the uncertainties in the anthropogenic emissions are neither spatially nor temporally correlated due to the heterogeneity of these emissions and the block is therefore diagonal. Each diagonal element is set at $(0.3)^2$: this σ value in the log-space corresponds to a factor ranging between 74%-135% in the emission space at the 1-day and model's grid scale. A second non-diagonal block is set for natural fluxes, accounting for space correlations in the uncertainties with a $\lambda_0 = 30$ km decorrelation length since these fluxes can be more spread and homogeneous in space than the anthropogenic emissions. On the diagonal, uncertainties are set to a value of $(0.6)^2$. This value σ in the log-space corresponds to a factor ranging between 55%-182% in the emission space at the 1-day and model's grid scale.

$$\mathbf{B} = \begin{pmatrix} \begin{pmatrix} \sigma_{ii}^{ant} & \dots & 0 \\ \vdots & \ddots & \vdots \\ 0 & \dots & \sigma_{jj}^{ant} \end{pmatrix} & \mathbf{0} \\ \mathbf{0} & \begin{pmatrix} \sigma_{j+1,j+1}^{bio} & \dots & \nu_{k,j+1}^{bio} \\ \vdots & \ddots & \vdots \\ \nu_{j+1,k}^{bio} & \dots & \sigma_{kk}^{bio} \end{pmatrix} \end{pmatrix} \tag{3}$$

https://doi.org/10.5194/egusphere-2024-103
Preprint. Discussion started: 19 February 2024

with ν of the form:

$\nu_{nm} = \sigma_n \sigma_m e^{\frac{-\Delta_x}{\lambda_0}}$

$\mathcal{H}$ is the observation operator, linking the control variables in the log-space to the simulated equivalents of the super-observations. It includes the exponential operator and scaling factor converting the maps of the logarithm of the coefficient for the emissions into emission maps at the spatial and temporal resolutions of CHIMERE, the atmospheric chemistry and transport model CHIMERE itself, and the extraction of the TVCDs from CHIMERE where and when we have TROPOMI super-observations. The uncertainties on the observations y and on the observation operator are characterized by the so-called observation error covariance matrix $\mathbf{R}$, set-up here as a diagonal matrix. The variance of the observation errors corresponding to individual observations in $\mathbf{R}$, set-up here as a diagonal matrix, is the quadratic sum of the error we have assigned to the TROPOMI-PAL super-observations (see Section 2.4), and of an estimate of the errors from the observation operator. We assume that the observation operator error is dominated by the chemistry-transport modeling errors and by the errors associated with the discrepancies between the spatial representativity of the super-observations and of the model corresponding column: it is set at 30% of the retrieval value. It was set at 20% by Fortems-Cheiney et al. (2021) at a coarser resolution and is increased here to take into account the mismatch between the shape and location of the real and simulated atmospheric patterns at our finer resolution (see Section 2.4).

The minimum of the cost function J is searched for with the iterative M1QN3 limited-memory quasi-Newton minimization algorithm (Gilbert and Lemaréchal, 1989). At each iteration, the computation of the gradient of J relies on the adjoint of the observation operator, and in particular on the adjoint of CHIMERE. In the results presented in Section 3, as a compromise between computational time and the level of convergence of the iterative minimization of J in the inversions, the minimization is considered to be satisfying when the norm of the gradient of J is reduced by 80%.

The calculation of the uncertainty in the posterior estimates of emissions is challenging when using a variational inverse system (Kadygrov et al., 2015; Rayner et al., 2019; Fortems-Cheiney et al., 2021) and it is not done here. It would require a large ensemble of time-consuming inversions (especially due to the handling of chemistry), to enable a proper sampling of the uncertainties and thus a proper derivation of the of the statistics of uncertainty.

https://doi.org/10.5194/egusphere-2024-103
Preprint. Discussion started: 19 February 2024

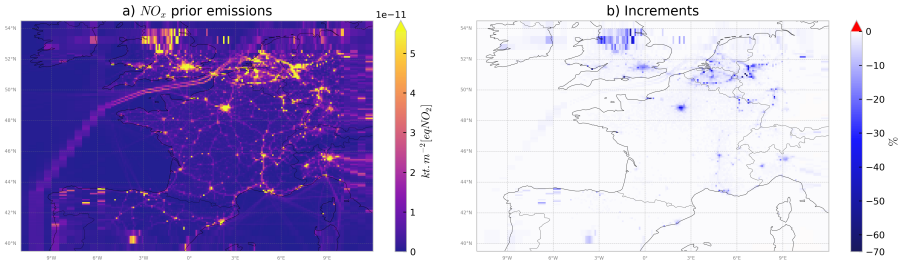

Figure 3. *a) NO_x total prior fluxes (anthropogenic emissions from CAMS-REG/INS and natural emissions from MEGAN, see Section 2.1 for details) and b) relative increments to the prior total emissions from the inversion in %, for April 2020.*

3 Results

3.1 Seasonal and inter-annual estimates of NO_x total French emissions

3.1.1 Fit between TROPOMI-PAL super-observations and their simulated equivalents

Before analyzing the results in terms of emissions, we check the behavior of the inversion by comparing the performances of the prior and posterior simulations in reproducing the spatial and temporal variations of the observations. As an illustration, TROPOMI-PAL and the corresponding CHIMERE NO_2 TVCDs are shown in 2a and Figure 2b, respectively, for April 2020. The TROPOMI-PAL observations and their NO_2 simulated equivalents present similar spatial patterns, with hotspots (TVCDs higher than $1\times10^{16}\,\mathrm{molec.cm^{-2}}$) over urban areas and low values over rural ones during the whole simulated period from 2019 to 2021 (illustrated in Figure 2a) and b) for one month in 2020). However, the prior simulation overestimates the NO_2 TVCDs over urban areas in France compared to the observations. For example, for April 2020, the mean bias between the prior simulation and TROPOMI is of about 4.2×10^{14}, 2.0×10^{14} and $3.8\times10^{14}\,\mathrm{molec.cm^{-2}}$ over Paris, Lyon and Marseille (Figure A1), respectively. The inversion brings the simulated TVCDs closer to the TROPOMI-PAL data over urban areas (Figure 2c): in this case, the mean bias and the mean RMS over the three cities are reduced by about 30% and 12% respectively.

As the CHIMERE prior simulation overestimates the NO_2 TVCDs, the inversion brings the CHIMERE NO_2 columns closer to the TROPOMI-PAL data by reducing NO_x emissions, mainly over dense urban areas (Ile-de-France, Lyon-Marseille axis, London area, Benelux, Frankfurt, Po Valley, see Figure 3b). Over these areas, the relative corrections provided by the inversions to the total (anthropogenic and natural) emissions can reach -70% (Figure 3b).

3.1.2 Estimates of NO_x French total emissions

This section focuses on the results from the NO_x inversions in terms of comparisons between the total (anthropogenic and natural) posterior NO_x emissions and the prior ones. At the national scale, both the prior and the posterior emissions present a similar seasonal cycle in 2019-2021, with emissions higher than 72 $\mathrm{kteqNO_2}$ during winter and emissions equal to or lower than 66 $\mathrm{kteqNO_2}$ during summer (Figure 4). The mean French national budget for the years 2019 to 2021 from the posterior

https://doi.org/10.5194/egusphere-2024-103
Preprint. Discussion started: 19 February 2024

Domain or region	Period	CAMS-REG/INS + MEGAN inventories	Posterior in 2019		Posterior in 2020		Posterior in 2021		Posterior 2020-2019	CITEPA 2020-2019	Posterior 2021-2020	CITEPA 2021-2020
		$\mathrm{kteqNO_2}$	$\mathrm{kteqNO_2}$	[%]	$\mathrm{kteqNO_2}$	[%]	$\mathrm{kteqNO_2}$	[%]	[%]	[%]	[%]	[%]
France	Annual	875	853	-3	852	-3	845	-3	0	-13	-1	+3
	Spring (MAM)	227	224	-1	222	-2	222	-2	-1	-21	0	+12
	March	78	76	-3	74	-5	75	-4	-2	-12	+1	+5
	April	77	76	-1	75	-4	74	-3	-2	-30	0	+23
	May	73	72	-1	73	-1	72	-1	+2	-22	-2	+10
	November	69	65	-6	67	-4	66	-4	+4	-19	-2	+14

Table 1. *Prior and posterior NO_x total emission budgets in* $\mathrm{kteqNO_2}$ *and their relative differences in %* $[100(posterior - prior)/prior]$*, in France for different periods. Columns "Posterior* $year_n - year_{n-1}$*" and "CITEPA* $year_n - year_{n-1}$*" show the relative difference between* $year_n$ *and* $year_{n-1}$ *posterior fluxes and CITEPA in %* $[100(F_{year_n} - F_{year_{n-1}})/F_{year_{n-1}}]$.

total emission estimates is about 850 $\mathrm{kteqNO_2}$, which is lower than the total prior emissions estimated from the CAMS-REG/INS and MEGAN inventories (average of 875 $\mathrm{kteqNO_2}$, Figure 3, Table 1), with the largest reductions reaching about 8% during fall and winter. This is expected as public policies have led to regular reductions in the anthropogenic emissions between 2016 (the year of our CAMS-REG/INS inventory) to 2019-2021. The decrease in total NO_x emissions is estimated at -13% from 2016 to 2019 by the French Technical Reference Center for Air Pollution and Climate Change (CITEPA report, we use the estimates for "out-of-scope" natural emissions which are not reported to UNFCCC). According to the CITEPA, the reduction is driven by large reductions in emissions from three major sectors: the energy sector (-28%), the industry sector (-22%), and the transport sector (-15%) between 2016 and 2019. However, the decrease found in this work is only about -3% (Table 1). This can be explained by our configuration with no temporal correlation in our $\mathbf{B}$ matrix, leading to null or very small correction of the prior emissions from the inversions when the coverage of the country by TROPOMI super-observations is very sparse (Zheng et al., 2020). In this case, the posterior emissions remain close to the prior emission estimate and therefore, at their 2016 level (see Section 3.2.3).

The 2019-2021 inter-annual variability is smaller with our inversions (Table 1) than in the estimates from the CITEPA: the annual budget of the French total NO_x posterior emissions varies by less than 1% from year-to-year, while the CITEPA estimates a decrease of about 13% in 2020 compared to 2019, and an increase of about 3% in 2021 compared to 2020 (Table 1). The similar annual total emissions in 2019 and 2020 nevertheless overlay different sub-annual variations. Higher emissions — partly associated with higher TROPOMI NO_2 tropospheric columns (not shown) — are estimated in January, in February, in June and in November 2020 compared to 2019 (Figure 4). These increases counterbalance the decrease of NO_x emissions in March and April 2020 (Figure 4, Figure 5) which could be both associated with the COVID-19 crisis and to meteorological conditions with a warmer winter in 2020 than in 2019 (see Section 3.2.2).

https://doi.org/10.5194/egusphere-2024-103
Preprint. Discussion started: 19 February 2024

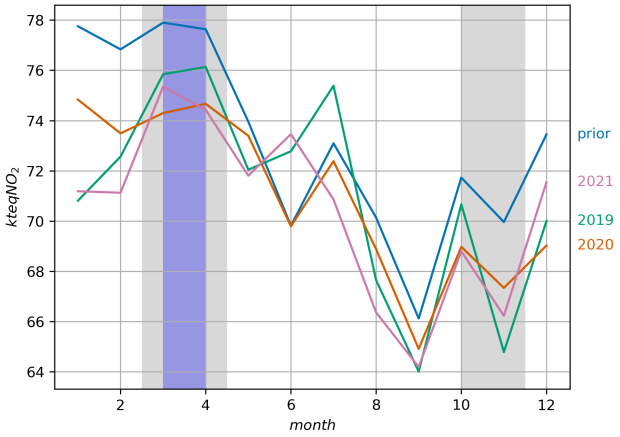

Figure 4. *Monthly NO_x total emissions in France as estimated by the CAMS-REG/INS and MEGAN inventories in 2016 (in blue) and by the inversions for years 2019 (in green), 2020 (in orange) and 2021 (in pink), in* $\mathrm{kteqNO_2}$*/month. Grey shaded areas show the French lockdown periods for the year 2020 and the purple shaded area shows the French lockdown period for the year 2021.*

3.2 Impact of the COVID-19 lockdown in spring 2020

The atmospheric lifetime of NO_2 dictates that the high spatial resolution measurements from TROPOMI should readily capture rapid week-to-week changes in near-surface emissions (Levelt et al., 2022) and should therefore make it possible to assess the impact of the COVID-19 lockdown in spring 2020 on NO_x French emissions. Following a usual diagnostic in the literature to assess the change in air pollutant concentrations due to the COVID-19 policies, we characterize the impact of the first COVID-19 lockdown in France — occurring from March 17^{th} to May 10^{th} 2020 — in terms of changes from spring 2019 to spring 2020.

3.2.1 General impact on NO_2 TROPOMI TVCDs

The TROPOMI NO_2 TCVDs in March and April 2020 are first compared to 2019 at the national scale (Table 2). The TROPOMI NO_2 TCVDs decrease from 2019 to 2020 by -11 and -28%, respectively in March and April over France. Similar decreases have been diagnosed in the measurements at surface stations over Europe with reductions in the average concentrations of NO_2 of about -25% for at least 75% of the 1308 European Air Quality e-Reporting database (AirBase) stations compared with the average of the previous seven years (2013–2019) for the period March 18–May 18, 2020 (Deroubaix et al., 2021). The population distribution is heterogeneous in France, with large rural areas (i.e., 75.7% of the country area, according to the French National Institute of Statistics and Economic Studies, 2020). We focus here on 8 urban areas which correspond to hotspots of NO_x concentrations, and where, as a consequence, we expect a stronger signal due to changes in anthropogenic activities (Figure A1): Paris, Lyon, Marseille, Lille, Bordeaux, Toulouse, Nice and Nantes. The population densities of these urban areas are given in Table A1. TROPOMI NO_2 tropospheric columns in March and April 2020 are 26 to 38% lower on

https://doi.org/10.5194/egusphere-2024-103
Preprint. Discussion started: 19 February 2024

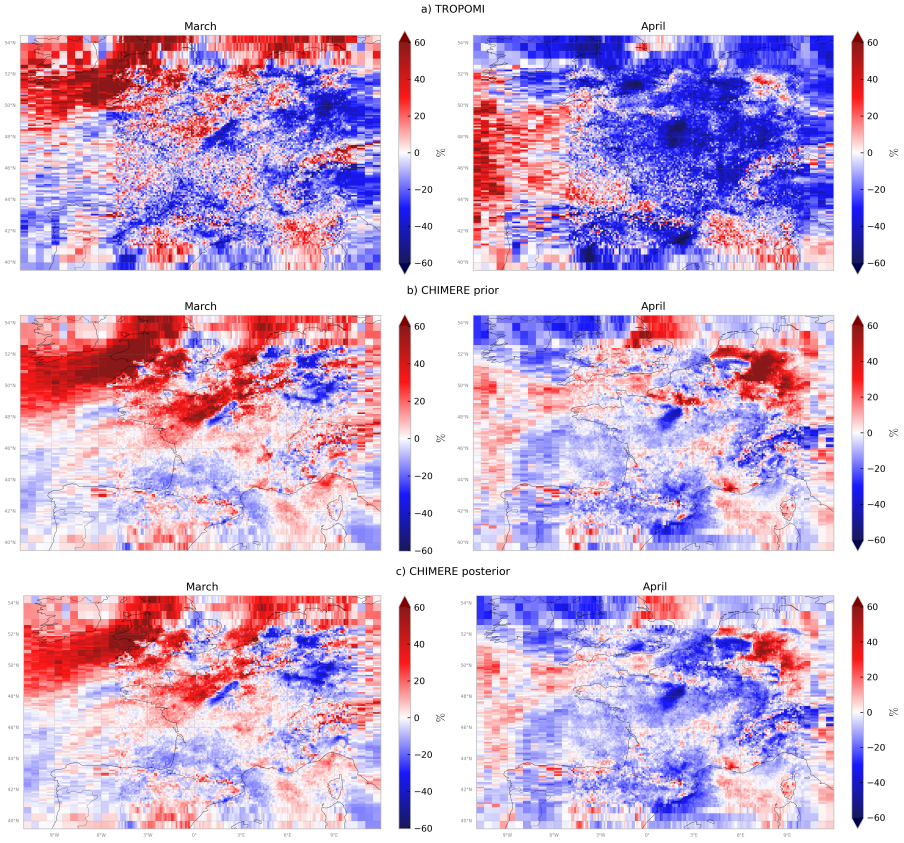

Figure 5. *Monthly gridded relative differences between monthly averages of a) TROPOMI-PAL NO_2 tropospheric columns, b) CHIMERE prior tropospheric columns and c) CHIMERE posterior tropospheric columns estimated by the inversions in 2020 and in 2019, for the months of March/April, in %* $[100(F_{2020} - F_{2019})/F_{2019})]$.

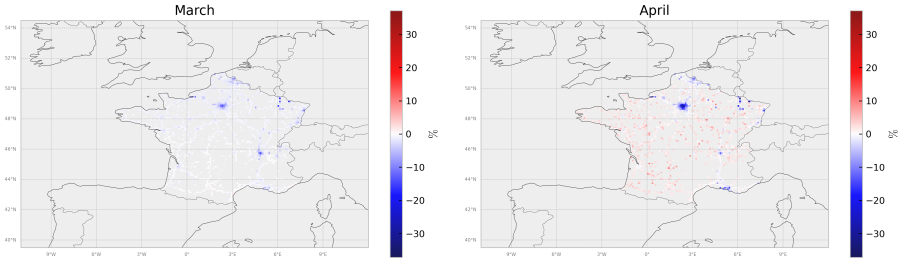

Figure 6. *Monthly gridded relative differences between the monthly total (anthropogenic + natural) posterior emissions estimated by the inversions from March/April 2019 to March/April 2020, for the months of March/April, using a urban and road land-use proxy (see Figure C1), in %* $[100(F_{2020} - F_{2019})/F_{2019}]$.

https://doi.org/10.5194/egusphere-2024-103
Preprint. Discussion started: 19 February 2024

Urban area	TROPOMI TVCD		CHIMERE prior TVCD		CHIMERE posterior TVCD		Emissions posterior	
	Mar	Apr	Mar	Apr	Mar	Apr	Mar	Apr
France	-11	-28	+7	-4	+2	-12	-2	-1
Bordeaux	-34	-27	-14	+23	-15	+21	-3	-1
Lille	-15	-35	+19	-10	+4	-28	-9	-11
Lyon	-27	-43	+13	+18	+1	+1	-15	-13
Marseille	-20	-27	-2	+46	-9	+19	-2	-7
Nantes	+2	-45	+16	-2	+14	-7	-3	-3
Nice	-28	-37	0	+7	-3	+2	0	-1
Paris	-41	-54	-4	+42	-12	-9	-11	-26
Toulouse	-41	-31	-23	-23	-22	-22	0	+1

Table 2. *Changes in NO_2 TROPOMI-PAL and CHIMERE tropospheric columns (in %) and changes in NO_x total posterior emissions (in %), between 2020 and 2019 for March/April, for the 8 French urban areas displayed in Figure A1.*

average than in 2019 over the 8 urban areas (Table 2).

The relative changes from April 2019 to April 2020 range from -54% for Paris to -27% in Bordeaux (Table 2). This relative change over Paris is consistent with the decrease of -52% described by (Levelt et al., 2022) and with the decrease of about -56% estimated by the tropospheric NO_2 columns measured by two UV-Visible Système d'Analyse par Observation Zénithale instruments (SAOZ, Pazmiño et al. (2021)).

The temporal variability of the changes from spring 2019 to spring 2020 also differs from one urban area to another. Excepted for Bordeaux and Toulouse, the reductions of TVCDs are higher in April 2020 (Figure 6, Table 2) than in March 2020 (Figure 5, Table 2). This is consistent with the fact that the French population has been confined only from mid-March (i.e., on March 17^{th}) versus the whole of April in 2020.

3.2.2 Various factors contributing to the differences in concentrations from spring 2019 to spring 2020 beyond the lockdown

The relative changes in the TROPOMI TVCDs from spring 2019 to spring 2020 are partly due to COVID-19 lockdowns but they are also driven by the changes in the meteorological and atmospheric chemistry transport conditions (Menut et al., 2020; Diamond and Wood, 2020; Petetin et al., 2020; Barré et al., 2021; Gaubert et al., 2021; Deroubaix et al., 2021).

The differences from spring 2019 to spring 2020 in the simulated CHIMERE prior NO_2 TVCDs (Figure 5) are mainly due to changes in the meteorology and to a lesser extent to changes in the model boundary conditions and in the biogenic emissions (Section 2.2), as the prior anthropogenic emissions are the same in 2019 and in 2020 (Section 2.1).

https://doi.org/10.5194/egusphere-2024-103
Preprint. Discussion started: 19 February 2024

CHIMERE prior NO_2 TVCDs are 23% higher in March 2020 than in March 2019 in the Northern part of France, excepted for the plume of Paris. These changes have thus a sign which is opposite to the changes expected from the COVID-19 lockdowns. This is in agreement with the analysis of Gaubert et al. (2021), who have shown that when considering only the effect of meteorological variability, the level of NO_2 concentrations would have been high during the 15 March–14 April 2020 period compared to the average NO_2 concentrations at the same period over the five previous years (2015–2019) in the north-western part of France (i.e., Bretagne, Pays de la Loire, Normandie and Hauts-de-France regions, Figure 5).

CHIMERE prior NO_2 TVCDs are 4% lower in April 2020 than in April 2019 over almost the entire country (excepted above Paris and in the Rhone Valley). This is consistent with temperatures above seasonal values (by 3° C over France, ranking as the third warmest April on record) and to persistent anticyclonic conditions in April 2020 (MeteoFrance, 2022)).

CHIMERE posterior NO_2 TCVDs are about 12% lower in April 2020 than in April 2019 over almost the entire country (Figure 5, Table 2); a focus at the city scale shows a decrease of about 9% over Paris between April 2020 and April 2019 whereas the prior NO_2 TCVDs increase by about 42% (Table 2).

Finally, the meteorological conditions also have an impact on the availability of the satellite observations. Due to the more favorable meteorological conditions with less cloud coverage leading to an unusual clear sky period in April 2020 (Gaubert et al., 2021; Deroubaix et al., 2021), there is a higher number of TROPOMI observations in April 2020 than in March 2020 and than in 2019, particularly over the northeastern part of France (Figure C2 in Supplementary materials), that may allow for a better correction of the CHIMERE NO_2 TCVDs for this particular period (Section 3.2.3).

3.2.3 Impact on NO_x anthropogenic emissions from spring 2019 to spring 2020

At the French national scale, the total NO_x emission estimates from the inversions present their largest decrease during the first lockdown in March and April 2020 compared to 2019 (Figure 4). The emissions between May and September are similar in 2020 to 2019 (Figure 4), coinciding with the ease of restrictions. Nevertheless, the decrease of NO_x emissions from March and April 2019 to March and April 2020, of about -2% and -3% respectively at the national scale, is relatively flatter than the estimations found in the literature. For example, the CITEPA estimates reductions of about -12 and -30% (Table 1), respectively, from March and April 2019 to March and April 2020 at the French national scale. Meteorology with a warmer winter can explain part of the changes in emissions between 2019 and 2020 for business sectors such as the residential combustion (Barré et al., 2021; Guevara et al., 2023).

We thus analyze the impact of the COVID-19 policies in terms of differences in retrieved anthropogenic emission estimates from the inversion, from spring 2019 to spring 2020. For this, we focus on urban areas, assuming that the emissions in these pixels (see Figure A1 for the chosen locations) are almost entirely due to anthropogenic activities.

In our inversions, the changes are negative in 7 of the 8 chosen urban areas (Figure 6, Table 2), qualitatively consistent with the strong reduction in the intensity of vehicle traffic (Guevara et al., 2021, 2022). The changes are also negative for urban areas outside France in our domain (Table C2). The impact of the lockdown on NO_x anthropogenic emissions is very different from one urban area to another. The highest reductions are seen in Paris with about -26% in April 2020 compared to April 2019, followed by Lyon (-13%), and Lille (-11%, Table 2). Several urban areas only present a very small drop of emissions in spring

https://doi.org/10.5194/egusphere-2024-103
Preprint. Discussion started: 19 February 2024

2020 (Table 2, Figure 7) e.g. the French urban areas Bordeaux, Nice and Nantes. The Toulouse urban area even show a slight increase (+1%) in April 2020 compared to April 2019 (Table 2, Figure 7). The population density difference between those cities could explain part of such variability: Paris, Lyon, Lille and Marseille have the highest population density in France, Table A1). A dedicated study might be necessary to understand in details the inter-urban variability and is not done here as up-to-date local inventories are not available for every city, particularly smaller ones.

The reductions in the NO_x anthropogenic emissions from spring 2019 to spring 2020, while substantial, do not exhibit the same magnitude as the reductions in TROPOMI-PAL NO_2 TVCDs. This is expected because of the non-linearities between NO_x anthropogenic emissions and NO_2 TVCDs but also, due to the limitations and assumptions of the inversion itself.

3.2.4 Exploring limitations in our analysis

The corrections provided by the inversions to the prior emissions can be limited by the fact that the potential of TROPOMI to provide information is hampered by the cloud coverage. As already mentioned in Section 3.1.2, the correction of the prior emissions from the inversions can be null or very small when TROPOMI observations are not available. In this case, the posterior emissions remain close to the prior. We quantify this effect by selecting days when we have at least one super-observations over the pixel of the 8 urban areas of interest and extrapolating the retrieved emissions for this subset of days to the whole year, hereafter called "filtered emissions". The reductions in the NO_x anthropogenic filtered emissions from spring 2019 to spring 2020 are almost always higher than for the standard posterior emissions (e.g., -28% and -24% over Paris and over Lyon respectively for filtered emissions versus -26% and -13%, Table 3). These results with such a focus on days with the best coverage are in principle much closer to the changes in emissions estimated by the CITEPA.

The corrections provided by the inversions to the prior emissions are also highly dependent on the errors associated with the TROPOMI-PAL observations and with the CTM errors in $\mathbf{R}$. We illustrate this effect by performing an inversion without model errors in the covariance matrix $\mathbf{R}$, giving more weight to the satellite data and considering the model as perfect. The posterior NO_x emissions retrieved with this error set-up at the city scale show a higher reduction from spring 2019 to spring 2020 (Tables 3, B3), e.g., -31% and -25% over Paris and over Lyon when using all the available observation and -33% and -42% for filtered emissions compared to -26% and -13% for the reference emissions.

Filtered cases are only indicative as this approach necessitates extrapolating from a notably small sample (days with observations, 16 and 19 days in average for the studied French cities in March and April 2020).

To gain in emission representativity, we suggest exploring a fine tuning of the correlation in $\mathbf{B}$ (with optionally additional information on NO_2 concentrations like surface stations) to compensate when TROPOMI data availability is lower. Despite our hypothesis made in Section 2.5 on anthropogenic fluxes, this might be necessary in addressing national-wide NO_x emission monitoring with a high local resolution.

https://doi.org/10.5194/egusphere-2024-103
Preprint. Discussion started: 19 February 2024

Urban area	Standard posterior emissions		Filtered posterior emissions		Standard posterior emissions **R**-perfect-model		Filtered posterior emissions **R**-perfect-model	
	Mar	Mar	Mar	Mar	Mar	Apr	Mar	Apr
Bordeaux	-3	-1	-9	-2	-5	-4	-13	-7
Lille	-9	-11	-16	-11	-10	-15	-17	-13
Lyon	-15	-13	-24	-24	-15	-25	-22	-41
Marseille	-2	-7	-5	-9	-2	-10	-5	-13
Nantes	-3	-3	-2	-7	-5	-5	-6	-11
Nice	0	-1	-4	-3	-1	-4	-5	-7
Paris	-11	-26	-15	-28	-13	-31	-15	-32
Toulouse	0	+1	-1	+1	-1	+1	-4	-1

Table 3. *Changes in NO_x CHIMERE total posterior emissions for the standard (in %) and with a simplified observation error set-up (in %),* **R** *matrix without model error, see details in Section 3.2.3 from March/April 2019 to March/April 2020 taking into account different TROPOMI coverage for the 8 French urban areas displayed in Figure A1.*

https://doi.org/10.5194/egusphere-2024-103
Preprint. Discussion started: 19 February 2024

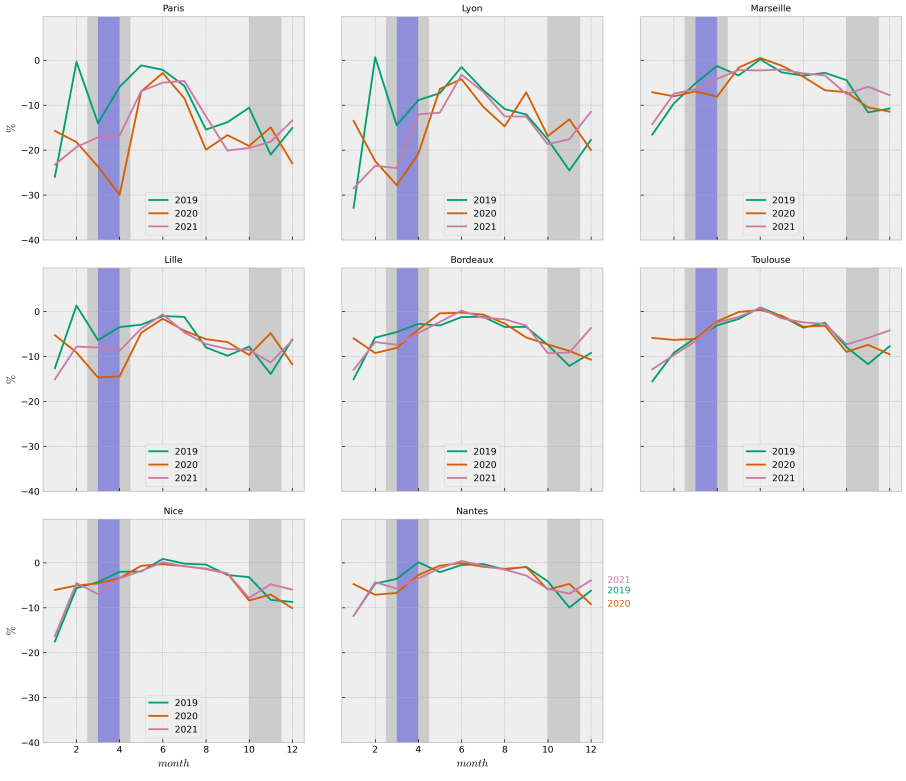

Figure 7. *NO_x anthropogenic emissions monthly budget relative differences between posterior and prior for the 8 French urban areas displayed in Figure A1, from inversion results for years 2019 (in green), 2020 (in orange) and 2021 (in pink), in %. Grey shaded areas show the French lockdowns periods for the year 2020 and the purple shaded area shows the French lockdown period for the year 2021.*

https://doi.org/10.5194/egusphere-2024-103
Preprint. Discussion started: 19 February 2024

4 Conclusions

We performed a three-year variational inversion of NO_x emissions from 2019 to 2021 in France at the high resolution of 10×10 km^2. The TROPOMI-PAL observations were assimilated within the inversion system CIF driving the regional CTM CHIMERE with the MELCHIOR-2 chemical scheme.

The French budgets for the years 2019, 2020 and 2021 are about 800 $kteqNO_2$. As expected from the implementation of public policies leading to regular reductions in emissions, these national budgets from the inversions are lower than the CAMS-REG/INS inventory for 2016, used as prior in our inversions. In particular, 2020 does not show a clear reduction in emission compared to 2019: 2020 emissions are higher compared to 2019 in January, February, June, and November. These increases dampen the decline in NO_x emissions in March and April 2020 compared to 2019.

We focus on the changes in NO_2 TROPOMI-PAL TVCDs and in NO_x anthropogenic emissions in March and April 2020 compared to 2019, that are due to the lockdowns during the COVID-19 pandemic and to meteorological conditions, including a milder winter (Barré et al., 2021; Guevara et al., 2023). Since inversions mainly detect changes in cities (hotspots), the main changes between March/April 2020 and 2019 are observed at the city scale. However, the impacts of restrictions can vary significantly between different urban areas. Among the 8 selected French urban areas, the relative changes between April 2020 and April 2019 in the TROPOMI-PAL observations ranges from -54% for Paris to -27% in Bordeaux. The highest reductions of NO_x anthropogenic emissions are seen in Paris with about -26% in April 2020 compared to April 2019, followed by Lyon (-13%), and Lille (-11%).

The corrections provided by the inversions to the prior emissions can be limited by the cloud coverage affecting the TROPOMI observations, and by errors in the TROPOMI data and in the CTM. Notably, when TROPOMI observations are unavailable, the correction of prior emissions in the unconstrained pixels through inversions is null, resulting in posterior emissions remaining close to the prior ones. Hence, the aggregation of posterior emissions into monthly or yearly budgets leads to a dampening of the signal provided by TROPOMI. To optimize the signal capture, emphasis is placed on days with at least one observation in the targeted pixels, yielding a more accurate estimate of the COVID-19 delta (higher reduction of NO_x anthropogenic emissions between spring 2019 and spring 2020).

To explore the impact of the set-up of error covariance matrices, we considered inversions without error models in the covariance matrix $\mathbf{R}$, giving more weight to satellite data. In this case, the posterior NO_x emissions at the city scale exhibit their highest reductions between spring 2020 and spring 2019 (e.g., -31% and -25% over Paris and over Lyon respectively). Assimilating the observations without accounting for the model error may lead to over-fitting and thus project the models errors onto the emission estimates. However, the weight of $\mathbf{R}$ in our inversions may have to be re-assessed with regards to the relatively conservative option that we use here to assign observation error to the super-observations. A finer assessment would require a good knowledge of the share of retrieval errors between randome noise without spatial correlations and more systematic errors with spatial correlations, as well as the typical length scales of such spatial correlations, which is currently challenging to derive (Miyazaki et al., 2012; Boersma et al., 2016; Lambert et al., 2023).

The emissions derived for cities are consistent with the existing literature but remain lower than most studies. In the absence of

https://doi.org/10.5194/egusphere-2024-103
Preprint. Discussion started: 19 February 2024

alternative information, like new measurements from benchmark cities, reconciling these results would prompt a re-evaluation of the observation errors in our inversion and a potential reassessment of our model error definition. The information contained in TROPOMI TCVDs cannot be fully exploited in our inversion set-up to get constraints on diffuse emissions e.g. in French rural areas. For emission hot-spots, addressing challenges arising from satellite coverage gaps may involve introducing horizontal, temporal, and sectoral correlations, although obtaining such high-resolution correlations poses a substantial challenge. Exploring corrections to parameters underlying inventories, such as Fossil Fuel Data Assimilation System (FFDAS) for CO_2, may offer a cleaner extrapolation. If achieved, these additions would assist the inversion system in implementing nationwide emission adjustments. Furthermore, the incorporation of a hypothetical geostationary satellite (such as Sentinel 4) in conjunction with ground-based monitoring stations, could enhance the temporal resolution and enable the capture of daily NO_x cycles, while also increasing the sensitivity of the satellite data near the surface.

Code availability. The CHIMERE code is available here: www.lmd.polytechnique.fr/chimere/, (Menut et al., 2013; Mailler et al., 2017). The CIF code is availbale here: http://community-inversion.eu/index.html (Berchet et al., 2021).

Data availability. The re-processed TROPOMI-PAL dataset is available on https://data-portal.s5p-pal.com (Eskes et al., 2021).

https://doi.org/10.5194/egusphere-2024-103
Preprint. Discussion started: 19 February 2024

Appendix A: Metropolitan masks

The list of all 15 urban areas and their masks is displayed on the following figure. Each mask is made out of $10 \times 10\ \mathrm{km}^2$ pixels.

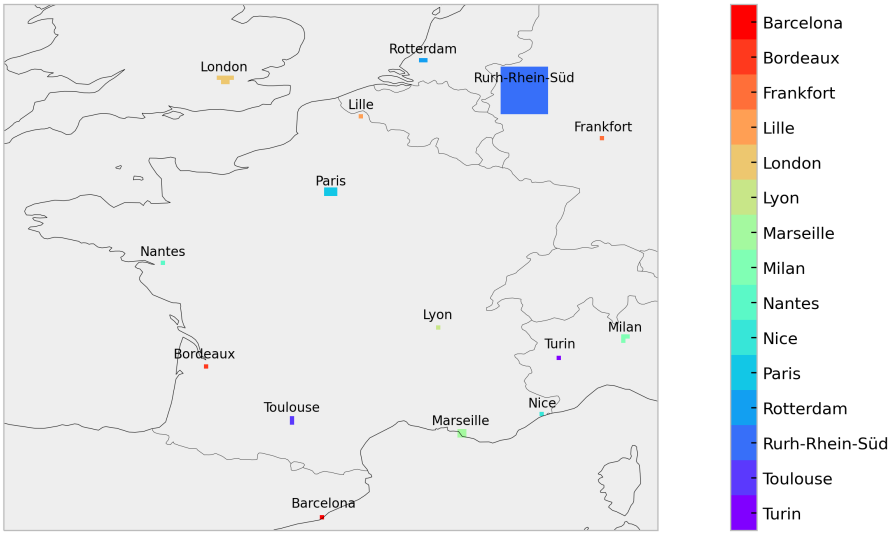

Figure A1. *Urban areas studied.*

https://doi.org/10.5194/egusphere-2024-103
Preprint. Discussion started: 19 February 2024

Urban area	Area [number of 10×10 km^2 pixels]	Population density [inhab.km^{-2}] EuroStat
Barcelona	1	723
Bordeaux	1	164
Frankfurt	1	633
Lille	1	455
London	6	1435
Lyon	1	580
Marseille	4	289
Milan	3	1591
Nantes	1	209
Nice	1	253
Paris	6	1025
Rotterdam	2	1092
Ruhr-Rhein-Süd	121	-
Toulouse	2	221
Turin	1	329

Table A1. *Cities studied in the paper and their areas in pixels with their population density according to EuroStat (statistics for 2019).*

https://doi.org/10.5194/egusphere-2024-103
Preprint. Discussion started: 19 February 2024

Appendix B: Additional tables

Domain or region	Period	CAMS-REG/INS + MEGAN inventories	Posterior in 2019		Posterior in 2020		Posterior in 2021		Posterior 2020-2019	CITEPA 2020-2019	Posterior 2021-2020	CITEPA 2021-2020
		$\mathrm{kteqNO_2}$	$\mathrm{kteqNO_2}$	[%]	$\mathrm{kteqNO_2}$	[%]	$\mathrm{kteqNO_2}$	[%]	[%]	[%]	[%]	[%]
Paris	Annual	27	24	-11	23	-17	23	-15	-6	-	+2	-
	Spring (MAM)	7	7	-7	6	-21	6	-14	-15	-	+9	-
	March	3	2	-14	2	-24	2	-17	-11	-	+9	-
	April	3	2	-6	2	-30	2	-17	-25	-	+19	-
	May	2	2	-1	2	-7	2	-7	-7	-	+1	-
	November	2	2	-21	2	-15	2	-18	+8	-	-4	-

Table B1. *Prior and posterior NO_x total emission budgets in* $\mathrm{kteqNO_2}$ *and their relative differences in* % $[100(posterior - prior)/prior]$, *in Paris for different periods. Columns "Posterior* $year_n - year_{n-1}$*" and "CITEPA* $year_n - year_{n-1}$*" show the relative difference between* $year_n$ *and* $year_{n-1}$ *posterior fluxes and CITEPA in* % $[100(F_{year_n} - F_{year_{n-1}})/F_{year_{n-1}}]$.

https://doi.org/10.5194/egusphere-2024-103
Preprint. Discussion started: 19 February 2024

Urban area	TROPOMI TVCD		CHIMERE prior TVCD		CHIMERE posterior TVCD		Emissions posterior	
	Mar	Apr	Mar	Apr	Mar	Apr	Mar	Apr
Barcelona	-42	-72	-13	-12	-20	-29	-4	-8
Bordeaux	-34	-27	-14	+23	-15	+21	-3	-1
Frankfurt	-54	+1	-18	+58	-25	+39	-7	-10
Lille	-15	-35	+19	-10	+4	-28	-9	-11
London	-7	-38	+4	+5	-3	-14	-5	-12
Lyon	-27	-43	+13	+18	+1	+1	-15	-13
Marseille	-20	-27	-2	+46	-9	+19	-2	-7
Milan	-30	-21	+28	+2	-8	-13	-13	-2
Nantes	+2	-45	+16	-2	+14	-7	-3	-3
Nice	-28	-37	0	+7	-3	+2	0	-1
Paris	-41	-54	-4	+42	-12	-9	-11	-26
Rotterdam	-35	-17	-15	+39	-19	+12	-5	-6
Ruhr-Rhein-Süd	-25	-9	-21	+42	-24	+8	-16	-26
Toulouse	-41	-31	-23	-23	-22	-22	0	+1
Turin	-33	-41	+17	-5	+1	-18	-1	-3

Table B2. *Changes in NO_2 TROPOMI-PAL and CHIMERE tropospheric columns (in %) and changes in NO_x total posterior emissions (in %), between 2020 and 2019 for March/April for the selection of urban areas displayed in Figure A1.*

https://doi.org/10.5194/egusphere-2024-103
Preprint. Discussion started: 19 February 2024

Urban area	Standard posterior emissions		Filtered posterior emissions		Standard posterior emissions $\mathbf{R}$-perfect-model		Filtered posterior emissions $\mathbf{R}$-perfect-model	
	Mar	Mar	Mar	Mar	Mar	Apr	Mar	Apr
Barcelona	-4	-8	-7	-16	-6	-13	-10	-23
Bordeaux	-3	-1	-9	-2	-5	-4	-13	-7
Frankfurt	-7	-10	-12	-17	-11	-21	-20	-36
Lille	-9	-11	-16	-11	-10	-15	-17	-13
London	-5	-12	-3	-18	-5	-16	-2	-23
Lyon	-15	-13	-24	-24	-15	-25	-22	-41
Marseille	-2	-7	-5	-9	-2	-10	-5	-13
Milan	-13	-2	-22	-11	-14	-4	-22	-14
Nantes	-3	-3	-2	-7	-5	-5	-6	-11
Nice	0	-1	-4	-3	-1	-4	-5	-7
Paris	-11	-26	-15	-28	-13	-31	-15	-32
Rotterdam	-5	-6	-6	-10	-5	-9	-3	-12
Ruhr-Rhein-Süd	-16	-26	-16	-26	-16	-31	-15	-31
Toulouse	0	+1	-1	+1	-1	+1	-4	-1
Turin	-1	-3	-10	-4	+1	-6	-7	-8

Table B3. *Changes in NO_x CHIMERE total posterior emissions for the standard (in %) and with a simplified observation error set-up (in %, $\mathbf{R}$ matrix without model error, see details in Section 3.2.3 from March/April 2019 to March/April 2020 taking into account different TROPOMI coverage for the selection of urban areas displayed in Figure A1.*

https://doi.org/10.5194/egusphere-2024-103
Preprint. Discussion started: 19 February 2024

Appendix C: Additional figures

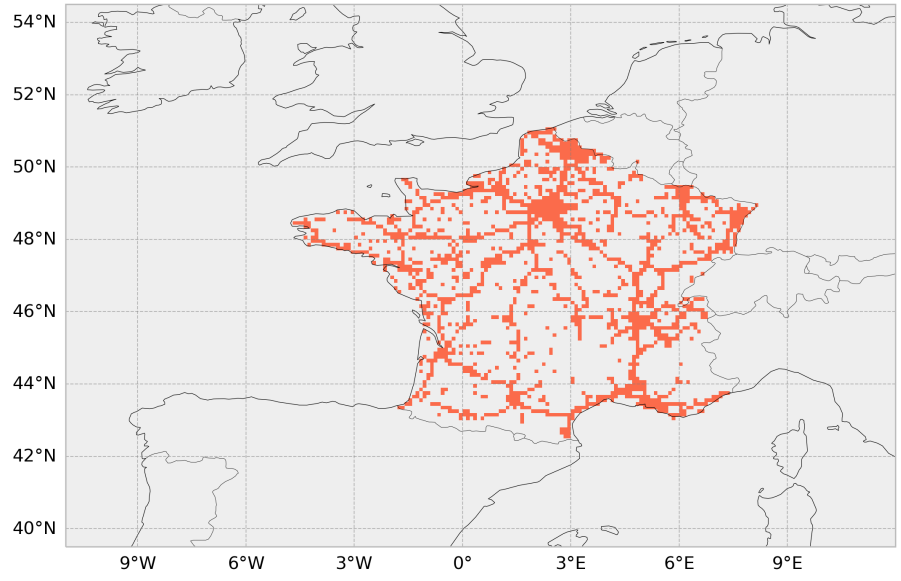

Figure C1. *Anthropogenic mask used over France using a urban and road land-use proxy.*

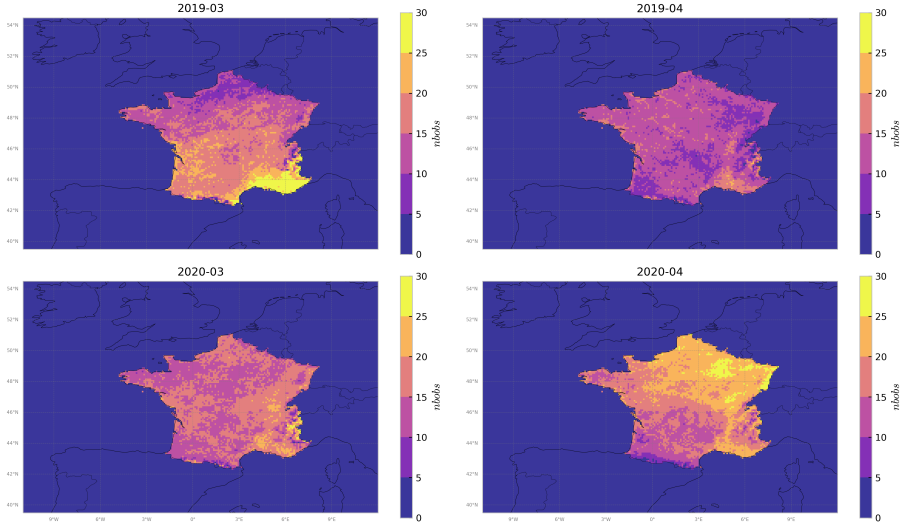

Figure C2. *Number of TROPOMI-PAL super-observations on the ARGFR domain in March/April 2019 and 2020.*

https://doi.org/10.5194/egusphere-2024-103
Preprint. Discussion started: 19 February 2024

Author contributions. RP, AFC, GB, IP, AB, EP, GD, AC, DS, and GS conceptualized the study. GS produced the prior emissions map. HE produced the satellite data. RP and AFC carried out inversions and data analysis. All co-authors contributed to the design of the study and to writing the manuscript.

Competing interests. The authors declare that they have no conflict of interest.

Acknowledgements. This study has received funding from the French ANR project ARGONAUT under grant agreement No ANR-19-CE01-0007 and from the French PRIMEQUAL project LOCKAIR under grant agreement No 2162D0010. This work was also supported by the CNES (Centre National d'Etudes Spatiales), in the frame of the TOSCA ARGOS project. This work was granted access to the HPC resources of TGCC under the allocations A0100102201 and A0110102201 made by GENCI. Finally, we wish to thank J. Bruna (LSCE) and his team for computer support.

https://doi.org/10.5194/egusphere-2024-103
Preprint. Discussion started: 19 February 2024

References

Barré, J., Petetin, H., Colette, A., Guevara, M., Peuch, V.-H., Rouil, L., Engelen, R., Inness, A., Flemming, J., Pérez García-Pando, C., Bowdalo, D., Meleux, F., Geels, C., Christensen, J. H., Gauss, M., Benedictow, A., Tsyro, S., Friese, E., Struzewska, J., Kaminski, J. W., Douros, J., Timmermans, R., Robertson, L., Adani, M., Jorba, O., Joly, M., and Kouznetsov, R.: Estimating lockdown-induced European NO_2 changes using satellite and surface observations and air quality models, Atmospheric Chemistry and Physics, 21, 7373–7394, https://doi.org/10.5194/acp-21-7373-2021, 2021.

Bauwens, M., Compernolle, S., Stavrakou, T., Müller, J.-F., Van Gent, J., Eskes, H., Levelt, P. F., Van Der A, R., Veefkind, J., Vlietinck, J., et al.: Impact of coronavirus outbreak on NO2 pollution assessed using TROPOMI and OMI observations, Geophysical Research Letters, 47, e2020GL087 978, 2020.

Berchet, A., Sollum, E., Thompson, R. L., Pison, I., Thanwerdas, J., Broquet, G., Chevallier, F., Aalto, T., Berchet, A., Bergamaschi, P., Brunner, D., Engelen, R., Fortems-Cheiney, A., Gerbig, C., Groot Zwaaftink, C. D., Haussaire, J.-M., Henne, S., Houweling, S., Karstens, U., Kutsch, W. L., Luijkx, I. T., Monteil, G., Palmer, P. I., van Peet, J. C. A., Peters, W., Peylin, P., Potier, E., Rödenbeck, C., Saunois, M., Scholze, M., Tsuruta, A., and Zhao, Y.: The Community Inversion Framework v1.0: a unified system for atmospheric inversion studies, Geoscientific Model Development, 14, 5331–5354, https://doi.org/10.5194/gmd-14-5331-2021, 2021.

Bieser, J., Aulinger, A., Matthias, V., Quante, M., and Van Der Gon, H. D.: Vertical emission profiles for Europe based on plume rise calculations, Environmental Pollution, 159, 2935–2946, 2011.

Boersma, K., Vinken, G., and Eskes, H.: Representativeness errors in comparing chemistry transport and chemistry climate models with satellite UV–Vis tropospheric column retrievals, Geoscientific Model Development, 9, 875–898, 2016.

Bovensmann, H., Burrows, J. P., Buchwitz, M., Frerick, J., Noël, S., Rozanov, V. V., Chance, K. V., and Goede, A. P. H.: SCIAMACHY: Mission Objectives and Measurement Modes, Journal of the Atmospheric Sciences, 56, 127–150, https://doi.org/https://doi.org/10.1175/1520-0469(1999)056<0127:SMOAMM>2.0.CO;2, 1999.

Brand, C.: Beyond 'Dieselgate': Implications of unaccounted and future air pollutant emissions and energy use for cars in the United Kingdom, Energy Policy, 97, 1–12, https://doi.org/10.1016/j.enpol.2016.06.036, 2016.

Burrows, J., Hölzle, E., Goede, A., Visser, H., and Fricke, W.: SCIAMACHY–scanning imaging absorption spectrometer for atmospheric chartography, Acta Astronautica, 35, 445–451, https://doi.org/10.1016/0094-5765(94)00278-t, earth Observation, 1995.

Burrows, J. P., Weber, M., Buchwitz, M., Rozanov, V., Ladstätter-Weißenmayer, A., Richter, A., DeBeek, R., Hoogen, R., Bramstedt, K., Eichmann, K.-U., Eisinger, M., and Perner, D.: The Global Ozone Monitoring Experiment (GOME): Mission Concept and First Scientific Results, Journal of the Atmospheric Sciences, 56, 151–175, https://doi.org/https://doi.org/10.1175/1520-0469(1999)056<0151:TGOMEG>2.0.CO;2, 1999.

Cao, X.-Q., Liu, B.-N., Liu, M.-Z., Peng, K.-C., and Tian, W.-L.: Variational principles for two kinds of non-linear geophysical KdV equation with fractal derivatives, Thermal Science, 26, 2505–2515, 2022.

Costa, S., Ferreira, J., Silveira, C., Costa, C., Lopes, D., Relvas, H., Borrego, C., Roebeling, P., Miranda, A., and Teixeira, J.: Integrating Health on Air Quality Assessment–Review Report on Health Risks of Two Major European Outdoor Air Pollutants: PM and NO_2, Journal of Toxicology and Environmental Health, pp. 307–340, https://doi.org/10.1080/10937404.2014.946164, 2014.

Derognat, C., Beekmann, M., Baeumle, M., Martin, D., and Schmidt, H.: Effect of biogenic volatile organic compound emissions on tropospheric chemistry during the Atmospheric Pollution Over the Paris Area (ESQUIF) campaign in the Ile-de-France region, Journal of Geophysical Research: Atmospheres, 108, 2003.

https://doi.org/10.5194/egusphere-2024-103
Preprint. Discussion started: 19 February 2024

Deroubaix, A., Brasseur, G., Gaubert, B., Labuhn, I., Menut, L., Siour, G., and Tuccella, P.: Response of surface ozone concentration to emission reduction and meteorology during the COVID-19 lockdown in Europe, Meteorological Applications, 28, e1990, 2021.

Diamond, M. S. and Wood, R.: Limited regional aerosol and cloud microphysical changes despite unprecedented decline in nitrogen oxide pollution during the February 2020 COVID-19 shutdown in China, Geophysical Research Letters, 47, e2020GL088 913, 2020.

Ding, J., Miyazaki, K., van der A, R. J., Mijling, B., Kurokawa, J.-i., Cho, S., Janssens-Maenhout, G., Zhang, Q., Liu, F., and Levelt, P. F.: Intercomparison of NO_x emission inventories over East Asia, Atmospheric Chemistry and Physics, 17, 10 125–10 141, https://doi.org/10.5194/acp-17-10125-2017, publisher: Copernicus GmbH, 2017.

Douros, J., Eskes, H., Geffen, J., Boersma, K., Compernolle, S., Pinardi, G., Blechschmidt, A.-M., Peuch, V.-H., Colette, A., and Veefkind, P.: Comparing Sentinel-5P TROPOMI NO2 column observations with the CAMS regional air quality ensemble, Geosci, Model Dev, 16, 509–534, https://doi.org/10.5194/gmd-16-509-2023, 2023.

Ebel, A., Friedrich, R., and Rodhe, H.: GENEMIS: Assessment, improvement, and temporal and spatial disaggregation of European emission data, Tropospheric Modelling and Emission Estimation: Chemical Transport and Emission Modelling on Regional, Global and Urban Scales, pp. 181–214, 1997.

EEA: Air quality in Europe – 2020 report, Tech. rep., European Union, ISBN 978-92-9480-292-7, https://doi.org/10.2800/786656, 2020.

EEA: Europe's air quality status 2023, Eea report, EEA, https://www.eea.europa.eu/publications/europes-air-quality-status-2023, 2023.

Elbern, H., Schmidt, H., Talagrand, O., and Ebel, A.: 4D-variational data assimilation with an adjoint air quality model for emission analysis, Environmental Modelling & Software, 15, 539–548, 2000.

Elguindi, N., Granier, C., Stavrakou, T., Darras, S., Bauwens, M., Cao, H., Chen, C., Denier van der Gon, H. A. C., Dubovik, O., Fu, T. M., Henze, D. K., Jiang, Z., Keita, S., Kuenen, J. J. P., Kurokawa, J., Liousse, C., Miyazaki, K., Müller, J.-F., Qu, Z., Solmon, F., and Zheng, B.: Intercomparison of Magnitudes and Trends in Anthropogenic Surface Emissions From Bottom-Up Inventories, Top-Down Estimates, and Emission Scenarios, Earth's Future, 8, e2020EF001 520, https://doi.org/10.1029/2020ef001520, e2020EF001520 2020EF001520, 2020.

Eskes, H., van Geffen, J., Sneep, M., Veefkind, P., Niemeijer, S., and Zehner, C.: S5P Nitrogen Dioxide v02. 03.01 intermediate reprocessing on the S5P-PAL system: Readme file, 2021.

Eskes, H. J. and Boersma, K. F.: Averaging kernels for DOAS total-column satellite retrievals, Atmospheric Chemistry and Physics, 3, 1285–1291, https://doi.org/10.5194/acp-3-1285-2003, 2003.

Fortems-Cheiney, A., Pison, I., Broquet, G., Dufour, G., Berchet, A., Potier, E., Coman, A., Siour, G., and Costantino, L.: Variational regional inverse modeling of reactive species emissions with PYVAR-CHIMERE-v2019, Geoscientific Model Development, 14, 2939–2957, https://doi.org/10.5194/gmd-14-2939-2021, 2021.

Gaubert, B., Bouarar, I., Doumbia, T., Liu, Y., Stavrakou, T., Deroubaix, A., Darras, S., Elguindi, N., Granier, C., Lacey, F., et al.: Global changes in secondary atmospheric pollutants during the 2020 COVID-19 pandemic, Journal of Geophysical Research: Atmospheres, 126, e2020JD034 213, 2021.

Gilbert, J. and Lemaréchal, C.: Some numerical experiments with variable storage quasi Newton algorithms, Math. Program., 45, 407–435, https://doi.org/10.1007/bf01589113, 1989.

Guenther, A., Karl, T., Harley, P., Wiedinmyer, C., Palmer, P. I., and Geron, C.: Estimates of global terrestrial isoprene emissions using MEGAN (Model of Emissions of Gases and Aerosols from Nature), Atmospheric Chemistry and Physics, 6, 3181–3210, https://doi.org/10.5194/acp-6-3181-2006, 2006.

https://doi.org/10.5194/egusphere-2024-103
Preprint. Discussion started: 19 February 2024

Guevara, M., Jorba, O., Soret, A., Petetin, H., Bowdalo, D., Serradell, K., Tena, C., Denier van der Gon, H., Kuenen, J., Peuch, V.-H., and Pérez García-Pando, C.: Time-resolved emission reductions for atmospheric chemistry modelling in Europe during the COVID-19 lockdowns, Atmospheric Chemistry and Physics, 21, 773–797, https://doi.org/10.5194/acp-21-773-2021, 2021.

Guevara, M., Petetin, H., Jorba, O., Gon, H., Kuenen, J., Super, I., Jalkanen, J.-P., Majamäki, E., Johansson, L., Peuch, V.-H., and Pérez García-Pando, C.: European primary emissions of criteria pollutants and greenhouse gases in 2020 modulated by the Covid-19 pandemic disruptions, Earth Syst. Sci. Data, 14, 2521–2552, https://doi.org/10.5194/essd-14-2521-2022, 2022.

Guevara, M., Petetin, H., Jorba, O., Denier van der Gon, H., Kuenen, J., Super, I., Granier, C., Doumbia, T., Ciais, P., Liu, Z., Lamboll, R. D., Schindlbacher, S., Matthews, B., and Pérez García-Pando, C.: Towards near-real-time air pollutant and greenhouse gas emissions: lessons learned from multiple estimates during the COVID-19 pandemic, Atmospheric Chemistry and Physics, 23, 8081–8101, https://doi.org/10.5194/acp-23-8081-2023, 2023.

Henze, D. K., Seinfeld, J. H., and Shindell, D. T.: Inverse modeling and mapping US air quality influences of inorganic PM 2.5 precursor emissions using the adjoint of GEOS-Chem, Atmospheric Chemistry and Physics, 9, 5877–5903, 2009.

Kadygrov, N., Broquet, G., Chevallier, F., Rivier, L., Gerbig, C., and Ciais, P.: On the potential of the ICOS atmospheric CO 2 measurement network for estimating the biogenic CO 2 budget of Europe, Atmospheric Chemistry and Physics, 15, 12 765–12 787, 2015.

Kuenen, J. and Dore, C.: EMEP/EEA air pollutant emission inventory guidebook 2019: Uncertainties, Tech. rep., EEA, https://www.eea.europa.eu/publications/emep-eea-guidebook-2019/part-a-general-guidance-chapters/5-uncertainties, 2019.

Kuenen, J., Dellaert, S., Visschedijk, A., Jalkanen, J.-P., Super, I., and Gon, H.: CAMS-REG-v4: a state-of-the-art high-resolution European emission inventory for air quality modelling, Earth Syst. Sci. Data, 14, 491–515, https://doi.org/10.5194/essd-14-491-2022, 2022.

Lambert, J.-C., Keppens, A., Compernolle, S., Eichmann, K.-U., de Graaf, M., Hubert, D., Langerock, B., Ludewig, A., Sha, M., Verhoelst, T., Wagner, T., Ahn, C., Argyrouli, A., Balis, D., Chan, K., Coldewey-Egbers, M., Smedt, I. D., Eskes, H., Fjæraa, A., Garane, K., Gleason, J., Goutail, F., Granville, J., Hedelt, P., Ahn, C., Heue, K.-P., Jaross, G., Kleipool, Q., Koukouli, M., Lutz, R., Velarte, M. M., Michailidis, K., Nanda, S., Niemeijer, S., Pazmiño, A., Pinardi, G., Richter, A., Rozemeijer, N., Sneep, M., Zweers, D. S., Theys, N., Tilstra, G., Torres, O., Valks, P., van Geffen, J., Vigouroux, C., Wang, P., and Weber., M.: Quarterly Validation Report of the Copernicus Sentinel-5 Precursor Operational Data Products #21: April 2018 – November 2023, Tech. rep., CAMS Cluster Service, https://doi.org/S5P-MPC-IASB-ROCVR-21.01.00-20231218, 2023.

Lamsal, L. N., Martin, R. V., Padmanabhan, A., van Donkelaar, A., Zhang, Q., Sioris, C. E., Chance, K., Kurosu, T. P., and Newchurch, M. J.: Application of satellite observations for timely updates to global anthropogenic NOx emission inventories, Geophysical Research Letters, 38, https://doi.org/10.1029/2010gl046476, 2011.

Lattuati, M.: Impact des emissions Europeennes sur le bilan de l'ozone tropospherique a l'interface de l'Europe et de l'Atlantique Nord: apport de la modelisation Lagrangienne et des mesures en altitude, Ph.D. thesis, Paris 6, 1997.

Lee, S.-S., Chu, J.-E., Timmermann, A., Chung, E.-S., and Lee, J.-Y.: East Asian climate response to COVID-19 lockdown measures in China, Scientific reports, 11, 16 852, 2021.

Levelt, P., Stein Zweers, D., Aben, I., Bauwens, M., Borsdorff, T., Smedt, I., Eskes, H., Lerot, C., Loyola, D., Romahn, F., Stavrakou, T., Theys, N., Roozendael, M., Veefkind, J., and Verhoelst, T.: Air quality impacts of Covid-19 lockdown measures detected from space using high spatial resolution observations of multiple trace gases from Sentinel-5P/TROPOMI, Atmos, Chem. Phys, 22, 10 319–10 351, https://doi.org/10.5194/acp-22-10319-2022, 2022.

Levelt, P. F., Joiner, J., Tamminen, J., Veefkind, J. P., Bhartia, P. K., Stein Zweers, D. C., Duncan, B. N., Streets, D. G., Eskes, H., van der A, R., McLinden, C., Fioletov, V., Carn, S., de Laat, J., DeLand, M., Marchenko, S., McPeters, R., Ziemke, J., Fu, D., Liu, X., Pickering,

https://doi.org/10.5194/egusphere-2024-103
Preprint. Discussion started: 19 February 2024

K., Apituley, A., González Abad, G., Arola, A., Boersma, F., Chan Miller, C., Chance, K., de Graaf, M., Hakkarainen, J., Hassinen, S., Ialongo, I., Kleipool, Q., Krotkov, N., Li, C., Lamsal, L., Newman, P., Nowlan, C., Suleiman, R., Tilstra, L. G., Torres, O., Wang, H., and Wargan, K.: The Ozone Monitoring Instrument: overview of 14 years in space, Atmospheric Chemistry and Physics, 18, 5699–5745, https://doi.org/10.5194/acp-18-5699-2018, 2018.

Lin, J.-T.: Satellite constraint for emissions of nitrogen oxides from anthropogenic, lightning and soil sources over East China on a high-resolution grid, Atmospheric Chemistry and Physics, 12, 2881–2898, https://doi.org/10.5194/acp-12-2881-2012, 2012.

Mailler, S., Menut, L., Khvorostyanov, D., Valari, M., Couvidat, F., Siour, G., Turquety, S., Briant, R., Tuccella, P., Bessagnet, B., Colette, A., Létinois, L., Markakis, K., and Meleux, F.: CHIMERE-2017: from urban to hemispheric chemistry-transport modeling, Geoscientific Model Development, 10, 2397–2423, https://doi.org/10.5194/gmd-10-2397-2017, 2017.

Menut, L., Goussebaile, A., Bessagnet, B., Khvorostiyanov, D., and Ung, A.: Impact of realistic hourly emissions profiles on air pollutants concentrations modelled with CHIMERE, Atmospheric environment, 49, 233–244, 2012.

Menut, L., Bessagnet, B., Khvorostyanov, D., Beekmann, M., Blond, N., Colette, A., Coll, I., Curci, G., Foret, G., Hodzic, A., Mailler, S., Meleux, F., Monge, J.-L., Pison, I., Siour, G., Turquety, S., Valari, M., Vautard, R., and Vivanco, M. G.: CHIMERE 2013: a model for regional atmospheric composition modelling, Geoscientific Model Development, 6, 981–1028, https://doi.org/10.5194/gmd-6-981-2013, 2013.

Menut, L., Bessagnet, B., Siour, G., Mailler, S., Pennel, R., and Cholakian, A.: Impact of lockdown measures to combat Covid-19 on air quality over western Europe, Science of the Total Environment, 741, 140 426, 2020.

MeteoFrance: Bilan climatique du printemps 2020, Meteo france report, MeteoFrance, https://meteofrance.fr/sites/meteofrance.fr/files/files/editorial/bilan%5Fdefinitif%5Fprintemps%5F2020.pdf, 2022.

Mijling, B. and van der A, R. J.: Using daily satellite observations to estimate emissions of short-lived air pollutants on a mesoscopic scale, Journal of Geophysical Research: Atmospheres, 117, https://doi.org/10.1029/2012jd017817, 2012.

Mijling, B., van der A, R. J., and Zhang, Q.: Regional nitrogen oxides emission trends in East Asia observed from space, Atmospheric Chemistry and Physics, 13, 12 003–12 012, https://doi.org/10.5194/acp-13-12003-2013, 2013.

Miyazaki, K., Eskes, H. J., and Sudo, K.: Global NO_x emission estimates derived from an assimilation of OMI tropospheric NO_2 columns, Atmospheric Chemistry and Physics, 12, 2263–2288, https://doi.org/10.5194/acp-12-2263-2012, 2012.

Miyazaki, K., Eskes, H., Sudo, K., Boersma, K. F., Bowman, K., and Kanaya, Y.: Decadal changes in global surface NO_x emissions from multi-constituent satellite data assimilation, Atmospheric Chemistry and Physics, 17, 807–837, https://doi.org/10.5194/acp-17-807-2017, 2017.

Müller, J.-F. and Stavrakou, T.: Inversion of CO and NO_x emissions using the adjoint of the IMAGES model, Atmospheric Chemistry and Physics, 5, 1157–1186, https://doi.org/10.5194/acp-5-1157-2005, 2005.

Munro, R., Lang, R., Klaes, D., Poli, G., Retscher, C., Lindstrot, R., Huckle, R., Lacan, A., Grzegorski, M., Holdak, A., Kokhanovsky, A., Livschitz, J., and Eisinger, M.: The GOME-2 instrument on the Metop series of satellites: instrument design, calibration, and level 1 data processing – an overview, Atmospheric Measurement Techniques, 9, 1279–1301, https://doi.org/10.5194/amt-9-1279-2016, 2016.

Ordóñez, C., Garrido-Perez, J. M., and García-Herrera, R.: Early spring near-surface ozone in Europe during the COVID-19 shutdown: Meteorological effects outweigh emission changes, Science of the total environment, 747, 141 322, 2020.

Owens, R. G. and Hewson, T.: ECMWF Forecast User Guide, Tech. rep., ECMWF, https://doi.org/10.21957/m1cs7h, 2018.

https://doi.org/10.5194/egusphere-2024-103
Preprint. Discussion started: 19 February 2024

Pazmiño, A., Beekmann, M., Goutail, F., Ionov, D., Bazureau, A., Nunes-Pinharanda, M., Hauchecorne, A., and Godin-Beekmann, S.: Impact of the Covid-19 pandemic related to lockdown measures on tropospheric NO2 columns over Ile-de-France, Atmos, Chem. Phys, 21, 18 303–18 317, https://doi.org/10.5194/acp-21-18303-2021, 2021.

Petetin, H., Bowdalo, D., Soret, A., Guevara, M., Jorba, O., Serradell, K., and Pérez García-Pando, C.: Meteorology-normalized impact of the COVID-19 lockdown upon NO_2 pollution in Spain, Atmospheric Chemistry and Physics, 20, 11 119–11 141, https://doi.org/10.5194/acp-20-11119-2020, 2020.

Pison, I., Bousquet, P., Chevallier, F., Szopa, S., and Hauglustaine, D.: Multi-species inversion of CH 4, CO and H 2 emissions from surface measurements, Atmospheric Chemistry and Physics, 9, 5281–5297, 2009.

Quélo, D., Mallet, V., and Sportisse, B.: Inverse modeling of NOx emissions at regional scale over northern France: Preliminary investigation of the second-order sensitivity, Journal of Geophysical Research: Atmospheres, 110, 2005.

Rayner, P. J., Michalak, A. M., and Chevallier, F.: Fundamentals of data assimilation applied to biogeochemistry, Atmospheric Chemistry and Physics, 19, 13 911–13 932, https://doi.org/10.5194/acp-19-13911-2019, 2019.

Ritchie, H. and Roser, M.: Urbanization, Our world in data, 2018.

Savas, D., Dufour, G., Coman, A., Siour, G., Fortems-Cheiney, A., Broquet, G., Pison, I., Berchet, A., and Bessagnet, B.: Anthropogenic NOx Emission Estimations over East China for 2015 and 2019 Using OMI Satellite Observations and the New Inverse Modeling System CIF-CHIMERE, Atmosphere, 14, https://doi.org/10.3390/atmos14010154, 2023.

Siour, G., Colette, A., Menut, L., Bessagnet, B., Coll, I., and Meleux, F.: Bridging the scales in a eulerian air quality model to assess megacity export of pollution, Environmental modelling & software, 46, 271–282, 2013.

Souri, A. H., Chance, K., Bak, J., Nowlan, C. R., González Abad, G., Jung, Y., Wong, D. C., Mao, J., and Liu, X.: Unraveling Pathways of Elevated Ozone Induced by the 2020 Lockdown in Europe by an Observationally Constrained Regional Model: Non-Linear Joint Inversion of NO_x and VOC Emissions using TROPOMI, Atmospheric Chemistry and Physics Discussions, 2021, 1–45, https://doi.org/10.5194/acp-2021-121, 2021.

Stavrakou, T., Müller, J.-F., Boersma, K. F., van der A, R. J., Kurokawa, J., Ohara, T., and Zhang, Q.: Key chemical NO_x sink uncertainties and how they influence top-down emissions of nitrogen oxides, Atmospheric Chemistry and Physics, 13, 9057–9082, https://doi.org/10.5194/acp-13-9057-2013, 2013.

Stevens, C. J., David, T. I., and Storkey, J.: Atmospheric nitrogen deposition in terrestrial ecosystems: Its impact on plant communities and consequences across trophic levels, Functional Ecology, 32, 1757–1769, https://doi.org/10.1111/1365-2435.13063, 2018.

Szopa, S., Foret, G., Menut, L., and Cozic, A.: Impact of large scale circulation on European summer surface ozone and consequences for modelling forecast, Atmospheric Environment, 43, 1189–1195, 2009.

Valin, L., Russell, A., Hudman, R., and Cohen, R.: Effects of model resolution on the interpretation of satellite NO2 observations, Atmos, Chem. Phys, 11, 11 647–11 655, https://doi.org/10.5194/acp-11-11647-2011, 2011.

van der A, R. J., Eskes, H. J., Boersma, K. F., van Noije, T. P. C., Van Roozendael, M., De Smedt, I., Peters, D. H. M. U., and Meijer, E. W.: Trends, seasonal variability and dominant NOx source derived from a ten year record of NO2 measured from space, Journal of Geophysical Research: Atmospheres, 113, https://doi.org/10.1029/2007jd009021, 2008.

van Geffen, J., Eskes, H., Boersma, K., and Veefkind, J.: TROPOMI ATBD of the total and tropospheric NO_2 data products, Algorithm Theoretical Basis Document S5p-knmi-l2-0005-rp, KNMI, https://sentinels.copernicus.eu/documents/247904/2476257/Sentinel-5P-TROPOMI-ATBD-NO2-data-products, 2022a.

https://doi.org/10.5194/egusphere-2024-103
Preprint. Discussion started: 19 February 2024

van Geffen, J., Eskes, H., Compernolle, S., Pinardi, G., Verhoelst, T., Lambert, J.-C., Sneep, M., Linden, M., Ludewig, A., Boersma, K., and Veefkind, J.: Sentinel-5P TROPOMI NO2 retrieval: impact of version v2.2 improvements and comparisons with OMI and ground-based data, Atmos, Meas. Tech, 15, 2037–2060, https://doi.org/10.5194/amt-15-2037-2022, 2022b.

Veefkind, J., Aben, I., McMullan, K., Förster, H., de Vries, J., Otter, G., Claas, J., Eskes, H., de Haan, J., Kleipool, Q., van Weele, M., Hasekamp, O., Hoogeveen, R., Landgraf, J., Snel, R., Tol, P., Ingmann, P., Voors, R., Kruizinga, B., Vink, R., Visser, H., and Levelt, P.: TROPOMI on the ESA Sentinel-5 Precursor: A GMES mission for global observations of the atmospheric composition for climate, air quality and ozone layer applications, Remote Sensing of Environment, 120, 70–83, https://doi.org/10.1016/j.rse.2011.09.027, the Sentinel Missions - New Opportunities for Science, 2012.

Verhoelst, T., Compernolle, S., Pinardi, G., Lambert, J.-C., Eskes, H. J., Eichmann, K.-U., Fjæraa, A. M., Granville, J., Niemeijer, S., Cede, A., Tiefengraber, M., Hendrick, F., Pazmiño, A., Bais, A., Bazureau, A., Boersma, K. F., Bognar, K., Dehn, A., Donner, S., Elokhov, A., Gebetsberger, M., Goutail, F., Grutter de la Mora, M., Gruzdev, A., Gratsea, M., Hansen, G. H., Irie, H., Jepsen, N., Kanaya, Y., Karagkiozidis, D., Kivi, R., Kreher, K., Levelt, P. F., Liu, C., Müller, M., Navarro Comas, M., Piters, A. J. M., Pommereau, J.-P., Portafaix, T., Prados-Roman, C., Puentedura, O., Querel, R., Remmers, J., Richter, A., Rimmer, J., Rivera Cárdenas, C., Saavedra de Miguel, L., Sinyakov, V. P., Stremme, W., Strong, K., Van Roozendael, M., Veefkind, J. P., Wagner, T., Wittrock, F., Yela González, M., and Zehner, C.: Ground-based validation of the Copernicus Sentinel-5P TROPOMI NO_2 measurements with the NDACC ZSL-DOAS, MAX-DOAS and Pandonia global networks, Atmospheric Measurement Techniques, 14, 481–510, https://doi.org/10.5194/amt-14-481-2021, 2021.

Vinken, G. C. M., Boersma, K. F., van Donkelaar, A., and Zhang, L.: Constraints on ship NO_x emissions in Europe using GEOS-Chem and OMI satellite NO$_2$ observations, Atmospheric Chemistry and Physics, 14, 1353–1369, https://doi.org/10.5194/acp-14-1353-2014, 2014.

Visser, A. J., Boersma, K. F., Ganzeveld, L. N., and Krol, M. C.: European NO_x emissions in WRF-Chem derived from OMI: impacts on summertime surface ozone, Atmospheric Chemistry and Physics, 19, 11 821–11 841, https://doi.org/10.5194/acp-19-11821-2019, 2019.

Zheng, B., Geng, G., Ciais, P., Davis, S. J., Martin, R. V., Meng, J., Wu, N., Chevallier, F., Broquet, G., Boersma, F., van der A, R., Lin, J., Guan, D., Lei, Y., He, K., and Zhang, Q.: Satellite-based estimates of decline and rebound in China's CO_2 emissions during COVID-19 pandemic, Science Advances, 6, eabd4998, https://doi.org/10.1126/sciadv.abd4998, 2020.